

# S2TA: Exploiting Structured Sparsity for Energy-Efficient Mobile CNN Acceleration

Zhi-Gang Liu<sup>\*</sup>, Paul N. Whatmough<sup>\*</sup>, Yuhao Zhu<sup>+</sup>, and Matthew Mattina<sup>\*</sup>

<sup>\*</sup>Arm ML Research Lab, Boston, MA, USA, <sup>+</sup>University of Rochester, Rochester, NY, USA

## ABSTRACT

Exploiting sparsity is a key technique in accelerating quantized convolutional neural network (CNN) inference on mobile devices. Prior sparse CNN accelerators largely exploit unstructured sparsity and achieve significant speedups. Due to the unbounded, largely unpredictable sparsity patterns, however, exploiting unstructured sparsity requires complicated hardware design with significant energy and area overhead, which is particularly detrimental to mobile/IoT inference scenarios where energy and area efficiency are crucial.

We propose to exploit *structured* sparsity, more specifically, Density Bound Block (DBB) sparsity for both weights and activations. DBB block tensors bound the maximum number of non-zeros per block. DBB thus exposes statically predictable sparsity patterns that enable lean sparsity-exploiting hardware. We propose new hardware primitives to implement DBB sparsity for (static) weights and (dynamic) activations, respectively, with very low overheads.

Building on top of the primitives, we describe S2TA, a systolic array-based CNN accelerator that exploits joint weight and activation DBB sparsity and new dimensions of data reuse unavailable on the traditional systolic array. S2TA in 16nm achieves more than  $2\times$  speedup and energy reduction compared to a strong baseline of a systolic array with zero-value clock gating, over five popular CNN benchmarks. Compared to two recent non-systolic sparse accelerators, Eyerriss v2 (65nm) and SparTen (45nm), S2TA in 65nm uses about  $2.2\times$  and  $3.1\times$  less energy per inference, respectively.

## 1. INTRODUCTION

Convolutional neural network (CNN) inference has quickly become an important workload in (ultra) low-power mobile [11,42] and IoT/embedded [9,10,19] devices. CNN accelerators are now a standard component in mobile SoCs [16,37], where 8-bit integer (INT8) CNN inference is the most widely used [36] due to the stringent requirements on energy efficiency (TOPS/W) and area efficiency (TOPS/mm<sup>2</sup>).

A common strategy to improve CNN accelerator efficiency is to exploit sparsity, as zeros in the data tensors (both weights and activations) reduce the theoretical compute and storage requirement significantly. Zeros in CNNs are statistically distributed in a random pattern. Exploiting the random sparsity, which is also commonly referred to as *unstructured* sparsity, has been the main focus of sparse hardware accelerators to date [5, 12, 14, 27, 33]. Exploiting unstructured sparsity, however, requires complex hardware structures that introduce significant area and energy overhead, which are particularly detrimental to mobile/embedded inference scenarios.

Exploiting unstructured sparsity introduces hardware overheads due to additional buffers used in data manipulation. There are two fundamental approaches to supporting random sparsity. The first is the inner-product style [5, 35] which requires an *operand gather* stage to evenly distribute the unpredictable workload to the PEs to perform the MAC operations. The second, is the outer-product style which has more conventional operand distribution and MAC operations, but then requires a *result scatter* stage to spread the non-contiguous results of the individual MACs over the output feature maps. Both of these approaches introduce significant hardware overheads in the form of large buffers that drastically degrade the energy and area-efficiency of the accelerator.

We quantitatively show that the additional buffers required to exploit unstructured sparsity, which may seem like nitty-gritty engineering details, in fact increase the energy per MAC of a baseline (systolic array) dense accelerator by 71%. As a result, random sparse accelerators published to date have demonstrated high speedup, but due to hardware overheads, have limited energy and area efficiency gains.

We argue that the sparsity-exploiting microarchitecture structures must be lightweight for it to be beneficial to exploit sparsity at all in mobile/embedded CNN accelerators. Otherwise, the energy/area overheads can easily eclipse the speedup gains. To that end, we propose to exploit *structured sparsity*, which has regular sparsity patterns that allow the hardware additions required to be very lean. In particular, we focus on Density Bound Block (DBB) [18] format, which tiles data tensors into blocks, and then introduces a bound on the maximum number of non-zero elements per block. DBB overcomes both of the challenges with random sparsity. Firstly, the maximum number of MAC operations is fixed, which significantly achieves high PE utilization *without* operand buffers. Secondly, the blocked data limits the location of output results, eliding distributed accumulators.

We first propose two building primitives: W-DBB and A-DBB, which exploit DBB in weight sparsity and activation sparsity, respectively. Weight sparsity is statically known, and thus the hardware design is relatively straightforward. Activation sparsity, however, is dynamic. We propose a dynamic pruning scheme co-designed with a novel time-unrolled architecture to exploit DBB sparsity in activations.

Building on top of W-DBB and A-DBB, we describe how to integrate the two building blocks into a complete fully-sparse CNN accelerator that efficiently exploits sparsity in both weights and activations. In particular, we focus on the well-known systolic array architecture, which is popular in mobile/embedded inference scenarios due to its extreme

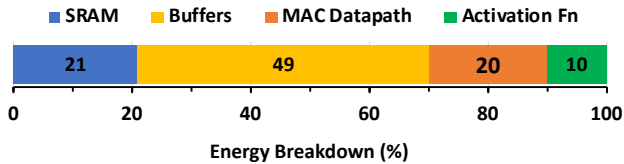


Figure 1: Energy breakdown for a conventional dense INT8 systolic array accelerator, for a typical CNN layer with 50% sparsity. The INT8 MAC datapath itself is very compact and consumes only 20% of the energy, while the operand and accumulator buffers dominate.

efficiency arising from high data reuse. We show that both W-DBB and A-DBB can be easily integrated into a classic SA architecture by introducing a tensor PE (TPE) design enabling further efficiency gains.

In summary, this paper makes the following contributions:

- Quantifying Overhead of Exploiting Unstructured Sparsity** We provide the first quantitative analysis of the hardware overhead, in terms of area and energy, of exploiting unstructured sparsity. We show that the additional operand and accumulator buffers, seemingly nitty-gritty engineering details, introduce about 50% and 10% area and energy overhead compared to a baseline dense INT8 CNN accelerator. These overheads are amortized in floating-point designs [24, 29, 35], where the datapath power is much higher, but in the mobile INT8 case, these overheads eclipse the gains.
- Joint Weight/Activation DBB Sparsity** We propose an architecture that exploits DBB sparsity in both weights and activations. This is non-trivial, because while weight sparsity is known offline, activation sparsity is not known until runtime and can vary wildly. We propose Dynamic Activation Pruning (DAP), which co-designs training time activation DBB pruning and novel run-time hardware support. DAP compresses activations by 2–3× with negligible impact on test accuracy.
- Time-Unrolled Variable DBB Sparsity** We propose a new time-unrolled microarchitecture to serialize the processing of MACs in a DBB block across time.
- Structured Sparse Tensor Accelerator (S2TA)** We show that joint DBB weight and activation sparsity can be efficiently incorporated into CNN accelerators. As a case study, we target the systolic array template, by extending the traditional scalar PE into a tensor PE (TPE) that consumes compressed DBB data blocks.
- Evaluation in 16nm and 65nm** We implement the S2TA design in both 16nm and 65nm technology. On a range of popular models (AlexNet, MobileNetv1, VGG-16, ResNet50v1), S2TA demonstrates 2.08× lower energy compared to the baseline without DBB. Compared to the state-of-the-art unstructured sparse accelerator SparTen [12] and Eyeriss-v2 [5], S2TA has 2.2× and 3.1× lower energy on AlexNet in 65nm technology.

## 2. MOTIVATION

In this section, we review the two fundamental approaches to supporting random sparsity in embedded CNN accelerators: (1) inner-product style with operand gather, and (2) outer-product style with result scatter. Both introduce significant hardware overheads that drastically degrade the energy and area-efficiency of the accelerator.

### 2.1 Sparsity-Exploiting Structures Must be Efficient for Mobile DNN Inference

The simplest way to exploit sparsity in hardware is Zero Value Clock Gating (ZVCG). Fig. 6b shows how ZVCG simply detects zero operands (weights and activations) and clock-gates the operand and/or result registers to reduce power dissipation. While ZVCG gives a significant reduction in datapath power [6, 30], it does not increase throughput, nor does it reduce the SRAM bandwidth (as the zeros are still stored and read in sequence). More importantly, ZVCG reduces the hardware utilization and, thus, does not improve area efficiency (TOPS/mm<sup>2</sup>), which is critical for mobile.

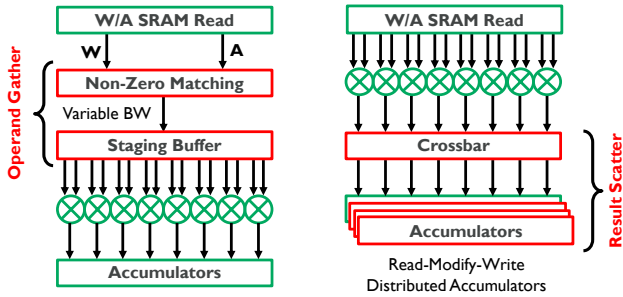
Sparse GEMM potentially achieves much higher gains than ZVCG by reducing both the number of MACs that need to be executed and also the memory bandwidth. To that end, only the non-zero values and a corresponding positional index are stored. The index encodes the position of each non-zero element in the expanded matrix, via either compressed sparse row/column (CSR/CSC) [14, 27] format or a simple bitmask [12]. At runtime, both the SRAM bandwidth, and the number of MACs executed are significantly reduced.

However, implementing fully sparse GEMM on energy and area-constrained INT8 mobile/IoT accelerators is challenging. Basically, removing MACs with zero operands breaks the regular compute pattern and requires complex on-chip buffering and data re-ordering to maximize the hardware utilization. The additional buffering structures significantly increase the energy and area overhead. Fig. 1 shows the energy breakdown of an INT8 dense systolic array accelerator for a typical CNN layer. The data is obtained from the extracted post-layout power estimation in a 16nm technology node with fully annotated switching activity.

**Key Insight** The energy consumption of the actual INT8 MAC computation in Fig. 1 is significantly overshadowed by the buffers used for operands and accumulators. Therefore, any sparsity-exploiting scheme must not introduce significant overheads that exacerbate the data buffering cost, as that is already the dominant energy consumer.

Today’s sparsity-exploiting mechanisms, unfortunately, introduce significant area and energy overhead for data buffering due to non-trivial data re-ordering, which can be classified into two fundamental categories, as illustrated in Fig. 2. The first category (Fig. 2a) performs a *gather* operation in the front-end to collect matching pairs of non-zero operands before buffering and finally performing MAC computations in the conventional manner. This approach is seen in previous work, including EIE [14], Eyerissv2 [5], and SMT-SA [35].

The second approach (Fig. 2b) avoids re-ordering operands in the front-end, by computing an outer-product (i.e. multiplying all non-zero weights with all non-zero activations). This approach is seen in accelerators such as SCNN [27] and SparTen [12]. However, this requires a *scatter* operation on the partial products using a very large number of read-modify-



(a) Inner-Product (Eyerissv2) (b) Outer-Product (SCNN)

Figure 2: Hardware structures for sparse GEMM require explicit data re-ordering, which introduces overheads (blocks in red), in the form of either (a) an operand gather stage before the MAC compute (SMT-SA [35]), or (b) a result scatter with a distributed accumulator (SCNN [27]).

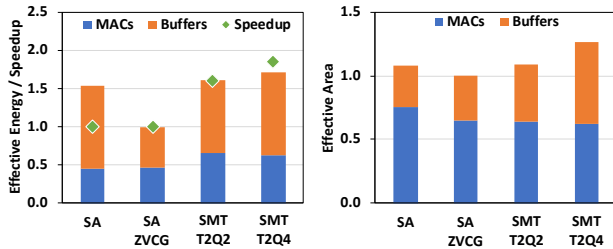


Figure 3: Effective energy/area and speedup, with breakdown by component for INT8 systolic array variants processing a typical convolution with 50% weight and activation sparsity. Energy and area are normalized by the effective throughput. The SMT, our INT8 re-implementation of [35], achieves speedup, but buffering overheads actually result in worse energy efficiency than even the dense case.

write accumulators to store the output activations.

The rest of this section quantifies the overhead associated with these two approaches.

## 2.2 Overhead 1: Operand Gather Structure

The weight ( $W$ ) and activation ( $A$ ) tensors have independent random sparsity patterns. Thus, during execution, we must walk the indexes to find matching pairs of non-zero positions to pass to the MAC units. For a fixed number of index pairs, the number of matches varies wildly depending on the position and the input data, which gives rise to an unpredictable number of MACs in any single cycle, leading to variable, unbalanced PE utilization at run time.

To keep the MAC utilization high, this load imbalance is usually evened out using a data staging buffer, which collects the matched operand pairs and packs them into groups of a fixed size that matches the datapath width [24, 29]. The hardware supporting this approach is shown in Fig. 2a. While the non-zero operand matching itself may be of a reasonable cost [12], the data staging buffer (typically FIFO) introduces high energy and area overheads, which are especially significant for low energy/area INT8 mobile/embedded accelerators.

Fig. 3 quantifies the energy and area overhead of the FIFOs used for distributing matching pairs for INT8 operands. We compare the energy and area across four designs: a dense

Table 1: Comparison of PE buffer sizes per INT8 MAC. Outer-product style accelerators (SCNN and SparTen) require large buffers per MAC compared to a baseline systolic array.

Architecture	Operands	Accumulators	Total
SCNN [27]	1.28 KB	0.375 KB	1.65 KB
SparTen [12]	864 B	128 B	0.99 KB
Eyeriss v2 [5]	165 B	40 B	205 B
SA-SMT <sup>1</sup> [35]	16 B	4 B	20 B
Systolic Array <sup>1</sup> [17]	2 B	4 B	6 B
S2TA-W <sup>2</sup> (Ours)	0.375 B	0.5 B	0.875 B
<b>S2TA-AW<sup>3</sup> (Ours)</b>	<b>0.75 B</b>	<b>4 B</b>	<b>4.75 B</b>

<sup>1</sup>Our INT8 version. <sup>2</sup>4/8 DBB 4×4×4\_4×8. <sup>3</sup>Time-Unrolled 8×4×4\_8×8, BZ=8

systolic array (SA), a systolic array with ZVCG optimization (SA-ZVCG), and two variants of SA-SMT, a recent systolic array that exploits random sparsity using operand FIFOs [35]. The two SA-SMT variants differ by their FIFO depths; one uses 2-entry FIFOs (SMT-T2Q2) and the other uses 4-entry FIFOs (SMT-T2Q4). The PPA is obtained for a typical convolution layer with 50% weight and activation sparsity. The energy and area are broken down into the two key SA components: MACs (compute) and the on-chip buffers.

**Key Insight** We find that the two SA-SMT variants achieve 1.6× and 1.8× speedup. However, this requires additional buffering for load balancing, introducing significant area and energy overheads. Overall, despite the speedup achieved, SMT shows nearly 50% higher power and roughly same area to SA-ZVCG, with INT8 operands required for mobile.

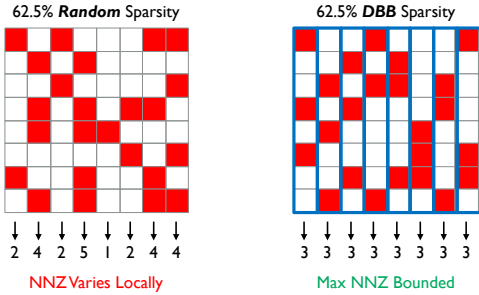
## 2.3 Overhead 2: Result Scatter Structure

A common alternative to the gather structure for matched operands, is to multiply every non-zero weight with every non-zero activation (i.e., an outer-product). In this approach, however, the MAC operations being executed in parallel correspond to different, typically non-contiguous elements in the output feature map. Therefore, the results of individual MACs must be properly distributed to the right elements in the output feature map, using a scatter operation.

Distributing the results is expensive because, instead of using a simple local output stationary accumulator register in the dense accelerator, one must construct a very large accumulator buffer using FF or SRAM, where each accumulator requires a read-modify-write operation to accumulate the partial sum in the correct place. The area and power overhead of this large accumulator buffer is, again, significant for INT8 inference accelerators, where the datapath logic is relatively cheap compared to the buffers (Fig. 1).

Tbl. 1 quantifies the overhead of the additional buffers that implement the result scatter function. Specifically, the table compares the buffer size per PE of the baseline systolic array and a range of different accelerators. Of these accelerators, SCNN [27] and SparTen [12] implement a scatter structure. While the systolic array requires only 2B for storing operands and 4B for storing the accumulators per PE, the storage requirement is significantly higher for other accelerators: e.g., SCNN [27] reports a total buffer size of 1.65 KB per PE, and SparTen [12] requires about 1 KB per PE.

## 3. MAIN IDEA AND DESIGN OVERVIEW



(a) Unstructured Sparse Tensor (b) DBB Sparse Tensor

Figure 4: Comparison of (a) an unstructured sparse tensor, and (b) a density bound block (DBB) sparse tensor. DBB constrains the maximum number of non-zeros (NNZ) per block, such that the max workload is known at design time. The NNZ shown is 3, and the block size (BZ) is 8.

This section first introduces the DBB structured sparsity, which we argue enables an efficient sparsity-exploiting architecture design (Sec. 3.1). We then highlight the rationale of our architecture support for DBB, with the detailed designs to follow in the subsequent sections (Sec. 3.2). Critically, all our DBB sparse architectures also support conventional dense operation for unpruned models.

### 3.1 Exploiting Structured Sparsity

The sparsity-exploiting structures must be lightweight to be at all beneficial in exploiting sparsity in mobile CNN accelerators. To that end, we propose to exploit *structured sparsity*, which has regular sparsity patterns that allow the hardware design to be lean. In particular, we focus on leveraging the Density Bound Block (DBB) sparsity. DBB essentially divides an (activation/weight) tensor into blocks and sets the upper bound of the number of non-zero (NNZ) elements in each block. Fig. 4 compares unstructured sparsity with DBB sparsity. While the overall sparsity level is the same, DBB sparsity constrains the maximum number of NNZs in a block such that the maximum workload is known at design time.

DBB provides two benefits. First, processing DBB blocks in order ameliorates the load imbalance problem and removes the distributed accumulator problem encountered with unstructured sparsity, avoiding the energy- and area-hungry buffers. Second, DBB lends itself to a simple hardware design based around the movement of small DBB data blocks, as we will illustrate with our S2TA accelerator (Sec. 6). This compact and efficient hardware architecture is possible because DBB results are naturally generated in sequential blocks; no data reordering or result index calculation is required.

Fig. 5 gives a concrete DBB example, where the block size (BZ) is  $8 \times 1$  and the maximum number of non-zero values (NNZ) per block is 4. In this particular example, the tensor blocking is performed along the channel dimension, which is a common strategy to avoid all the elements in any single channel falling into the same block. The compression itself has two steps. First, the non-zero elements are stored by removing the zeros. Second, a simple bitmask index  $M$  is added to encode the presence of a non-zero element at each location in the expanded block (size BZ).

We usually refer to a DBB block by the ratio  $NNZ/BZ$ .

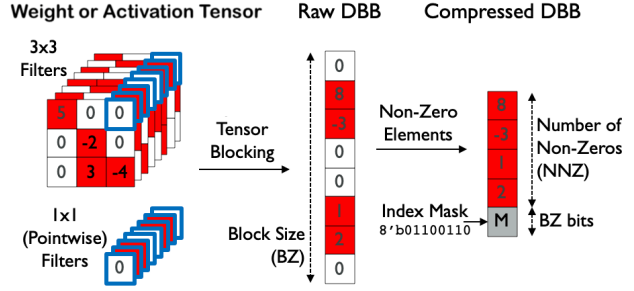


Figure 5: A 4/8 DBB example, where  $BZ=8$  and  $NNZ=4$ . The tensor is blocked along the channel dimension. The block is compressed by storing only the non-zero elements and their positional index bitmask ( $M$ ). The same compression applies to weights and activation tensors.

The example in Fig. 5 would be a 4/8 block. Note that any blocks that have less than NNZ non-zero elements will include one or more zeros in the compressed form. For sparse DBB execution, a block cannot contain more than NNZ non-zeros, achieved via pruning (Section 4 and 5). However, we also support a conventional dense mode for unpruned models.

### 3.2 Design Overview

The rest of the paper discusses how to build an efficient accelerator to exploit weight and activation DBB sparsity, without significant accuracy drop. Weight sparsity is statically known, and thus the hardware design is relatively straightforward. Activation sparsity, however, is dynamic. We propose a dynamic pruning scheme co-designed with a novel time-unrolled architecture to exploit DBB sparsity in activations.

Building on top of DBB compression for both weight and activation, we describe how to integrate them into a complete DNN accelerator (Sec. 6). In particular, we focus on the popular systolic architecture. We show that both weight and activation DBB support can be easily integrated into a classic SA architecture by grouping PEs, leading to a tensor PE (TPE) design. Critically, the TPE design naturally exposes additional dimensions of data reuse that is unobtainable in the traditional SA design, enabling further efficiency gains.

We note that weight DBB sparsity has been used in a commercial A100 GPU from Nvidia [25]. Our design differs in two ways. First, A100 supports only fixed 2/4 weight sparsity with up to  $2 \times$  speedup, while our design comprehensively exploits both weight and variable activation DBB sparsity for up to  $8 \times$  speedup using a novel time-unrolled architecture (Section 5.2). We show that activation DBB requires non-trivial extensions from previous weight DBB due to the dynamic nature of activation sparsity. Second, our design focuses on the systolic array architecture, which is well suited to low-power mobile/embedded systems. To fairly compare with A100, we implement an A100-featured systolic design, S2TA-W, as a baseline in the evaluation. Sec. 7 and 8.2.

## 4. STATIC WEIGHT DBB SPARSITY

This section describes an architecture to apply DBB to weight sparsity (W-DBB). We note that weight DBB has been explored in [18, 23, 40] and the proprietary A100 GPU from Nvidia with fixed 2/4 DBB [25, 28]. However, describing it

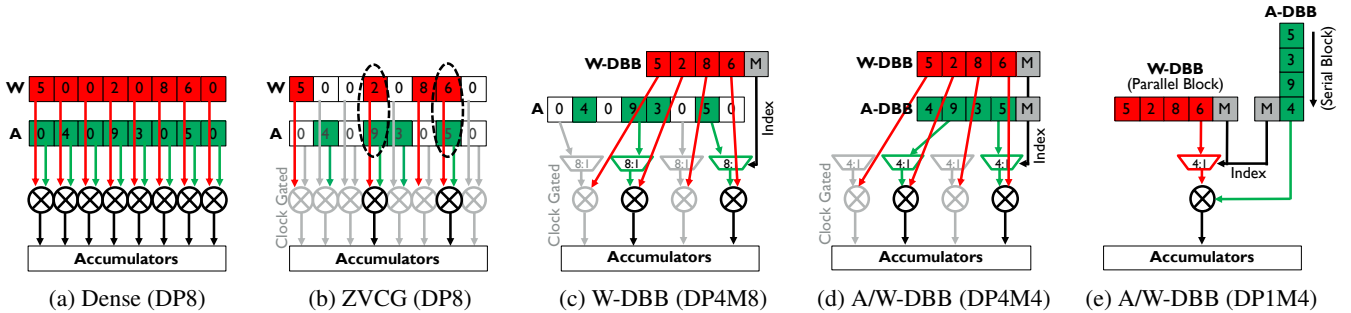


Figure 6: Parallel sparse MAC hardware. (a) Dense 8-MAC vector dot product (DP8). (b) Dense DP8 with zero-value clock gating (ZVCG) reduces power by exploiting random sparsity. (c) 4/8 weight DBB (W-DBB) sparsity uses only 4 MACs (DP4), with an 8:1 mux (M8) for each (DP4M8). (d) A/W-DBB uses a 4-way mux (DP4M4), but is limited to fixed DBB sparsity ratios. (e) W-DBB with Time-Unrolled, serialized A-DBB allows the hardware to support activation density from 1/8 to 8/8, tuned to the requirements of each layer. This is implemented with a very cheap single MAC and 4:1 mux (DP1M4).  $M$  denotes index bitmask.

allows us to explain the general principle of exploiting DBB, which we additionally leverage in activation DBB compression. As an additional insight, this design may help shed some light on Nvidia’s unpublished implementation [25].

The key advantage of weight DBB is that the load imbalance problem is greatly relaxed, as we have bounded the maximum number of non-zero elements per block and can provision hardware based on this. We illustrate this by modifying the simple parallel (vector) architecture template given in Fig. 6a, which show an 8-MAC dot product, which we refer to as DP8. Building on top of DP8, Fig. 6c shows a datapath for a 4/8 W-DBB block, using only 4 hardware MACs instead of 8, yielding a 50% reduction in MACs at the same throughput, and a 37.5% reduction in weight operand bandwidth. Since this design has only 4 MACs (DP4), with an 8-input mux (M8)<sup>1</sup>, we call this configuration DP4M8.

The key to the hardware for W-DBB is the 8:1 MUX in front of each MAC. The MUX is used to steer the correct activation element into the MAC, which is controlled by the positional bitmask ( $M$ ) from the weight DBB block. The overhead of this MUX is negligible, especially compared to the overhead required to exploit unstructured sparsity (Sec. 2). The DP4M8 (Fig. 6c) also easily accommodates fall back to conventional dense operation, which is essential to support models that have density greater than 50%. Note that the compressed weight DBB block could include zeros if the sparsity is very high, which we exploit using clock gating.

## 5. DYNAMIC ACTIVATION DBB SPARSITY

Activation DBB compression (A-DBB) can be used together with W-DBB, allowing us to exploit the full potential of sparse data, without significant overheads. However, A-DBB is more challenging than W-DBB because: (1) activation sparsity is unbounded, and (2) optimal activation DBB sparsity varies significantly across the layers of a network. In this section, we describe the co-designed Dynamic Activation Pruning (DAP) and time-unrolled variable DBB architecture to overcome these challenges.

### 5.1 Dynamic Activation Pruning (DAP)

<sup>1</sup>Omitting trivial reductions in mux widths for the sake of brevity.

While weights can be compressed ahead of time (offline), activations are the result of runtime computation and therefore must be compressed online. To do this, we propose Dynamic Activation Pruning (DAP), which prunes and compresses the dense activation tensors into the DBB format. The random sparsity of a given activation tensor may have more non-zeros in a block than allowed by the DBB  $NNZ$ . Therefore, DAP implements simple *Top-NNZ* pruning to keep the block elements with the largest magnitude. As with W-DBB (Fig. 5), the activation tensor is first decomposed into  $1 \times 1 \times BZ$  blocks along the channel dimension.

DAP is a lossy scheme, and can degrade test accuracy on some models if  $NNZ/BZ$  is small. For example, MobileNetV1 shows a test accuracy drop from 71% to 56.1% when using 4/8 DAP for all point-wise CNN layers. We propose an extension to the conventional DNN training procedure to make up any accuracy loss from DAP (Sec 8.1).

### 5.2 Architectural Support for A/W-DBB

**Basic Design** A simple implementation of joint DBB sparsity in a vector datapath is given in Fig. 6d, where both weights and activations are compressed to reduce operand bandwidth. As before, the only overheads are a single datapath multiplexer before each MAC, which this time is reduced to 4:1 (DP4M4). The index bitmasks can be trivially compared to determine matching non-zero positions, and unused MACs can be clock gated to further reduce power. Although this doesn’t increase utilization of MACs, both weight and activations are now compressed in DBB format, thus the power to load both from SRAM is decreased dramatically.

**Challenges to Support Variable A-DBB** However, Activation DBB introduces a significant challenge because the maximum sparsity varies significantly across layers, for example for ResNet50v1, the per-layer tuned activation DBB ranges from 8/8 (dense) in early layers down to 2/8 towards the end. Therefore, while weight density typically hovers below 50% and therefore 4/8 W-DBB is a safe choice, forcing a fixed activation DBB sparsity (A-DBB) would be a huge compromise and result in diminished gains. Therefore, in order to retain good gains from A-DBB, it is necessary to support *variable* A-DBB sparsity in the architecture.

Naively supporting variable DBB sparsity in hardware

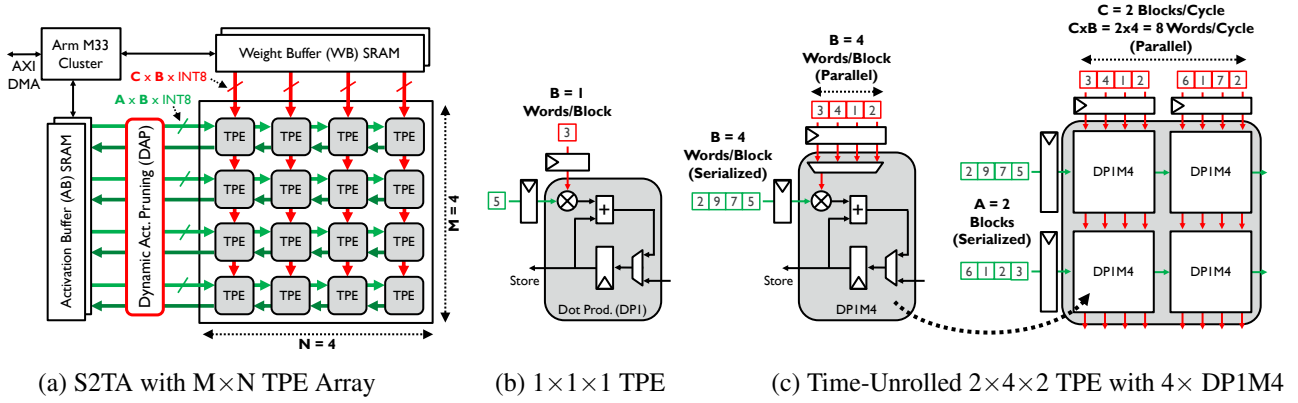


Figure 7: Overview of (a) S2TA accelerator with TPE array ( $N \times M$ ), dynamic activation pruning (DAP), local SRAM and Arm M33 MCUs. Example TPE configurations are denoted  $A \times B \times C$ , where  $B$  is the  $NNZ$  of the weight block.  $A$  is the number of activation operand block inputs per cycle, and  $C$  is the number of weight block inputs. TPE configs show for: (b) the classic scalar MAC PE ( $1 \times 1 \times 1$ ), (c) A Time-Unrolled  $2 \times 4 \times 2$  TPE implemented by connecting four DP1M4 units (Fig. 6e).

reduces utilization and leads to low energy and area efficiency. For example, if we implement a  $4/8$  DBB datapath and run a model with  $2/8$  DBB, the utilization would drop by  $\sim 50\%$ .

**Time Unrolled Architecture for Variable A-DBB** To support variable activation (A-DBB) sparsity efficiently, our key idea is to switch from unrolling the elements in the A-DBB blocks spatially (Fig. 6d) to serializing them in time (Fig. 6e). This simply means that we process one element of the activation block per cycle using a single MAC, over multiple cycles. For example, a layer with low density activations can use  $1/8$  DBB, requiring just one cycle per block. On the other hand, a layer with denser  $5/8$  DBB activations requires five cycles. In this way, we can now freely vary the activation block density ( $NNZ$ ) per layer directly by changing the number of cycles per block, from  $1/8$  to  $8/8$ . Meanwhile, the datapath utilization and operand bandwidth remain constant.

## 6. STRUCTURED SPARSE TENSOR ACCELERATOR (S2TA)

This section describes how to integrate the architectural support for W-DBB and variable A-DBB into a DNN accelerator to exploit weight and activation sparsity. As a case-study, we focus on systolic array-based DNN accelerators. Due to their superior efficiency arising from local register-to-register operand reuse [20], the systolic array has been widely promoted for CNN accelerators [21, 31, 32, 34, 35], and even used in commercial products [17]. We call our DBB-exploiting systolic array *S2TA*, with two main variants: (1) *S2TA-W* as a comparison baseline targeting W-DBB alone, and (2) our optimal time-unrolled *S2TA-AW* exploiting joint A/W-DBB.

### 6.1 Overall Architecture

The key to supporting DBB sparsity in a systolic array is to replace the traditional *scalar PE* with a *Tensor PE (TPE)*. A scalar PE (Fig. 7b) accepts a single pair of operands per cycle and computes a single MAC. A TPE (Fig. 7c), in contrast, accepts a pair of fixed size operand blocks per cycle.

TPE is a natural design choice to support DBB, since both weights and activations are naturally blocked in DBB. Each TPE essentially computes the MACs between an activation

tensor and a weight tensor. One can implement the TPE using the DP4M8 MAC unit in Fig. 6(c) to form *S2TA-W*. For the time-unrolled *S2TA-AW*, the DP1M4 MAC unit in Fig. 6(e) can be directly used as the TPE implementation.

A TPE can be configured in a variety of ways. For instance, Fig. 7(c) shows a TPE that accepts a weight tensor and an activation tensor in 4 cycles, with tensor size  $A \times B = 2 \times 4$  and  $B \times C = 4 \times 2$ , where  $B$  is essentially the  $NNZ$  of the weight DBB block. The degenerate case of a  $1 \times 1 \times 1$  TPE is equivalent to the scalar PE from a traditional SA (Fig. 7b). Fig. 7c shows a  $2 \times 4 \times 2$  TPE to exploit joint A/W-DBB, which internally is implemented by connecting four time-unrolled scalar DP1M4 datapath in Fig. 6(e) together in a pure outer-product fashion. In contrast, a TPE implemented with DP4M8 datapath (Fig. 6(c)) for exploiting W-DBB alone is reminiscent of a 4-way dot-product with dense  $A \times BZ$  activation and sparse  $B \times C$  weight tensor inputs to the TPE.

At the array level, TPEs operate in the usual systolic fashion as shown in Fig. 6a: each TPE receives a pair of tensor operands from adjacent neighbors and passes them on, except that the operands are tensors instead of scalar values. Networks are mapped onto the array using simple matrix tiling, similar to the TPU [17], except we use output-stationary.

**Data Reuse** In addition to naturally supporting DBB sparsity, the TPE organization exposes two new dimensions of data reuse compared to the  $1 \times 1 \times 1$  PE organization in classic systolic arrays. First, moving from a scalar MAC to a tensor-wise product in the TPE introduces *intra-TPE accumulator reuse*, as we now achieve multiple MACs per accumulator update<sup>2</sup>, but lower the chance of ZVCG. Second, moving from a single scalar input to tensors ( $A \times B \times C \neq 1$ ) introduces *intra-TPE operand reuse*, as each operand arriving at a TPE is used more than once. This amortizes the cost of moving operands across the array, amongst multiple MACs.

These two new forms of data reuse result in much smaller on-chip buffer sizes, as the flip-flops required in the TPE are increasingly shared amongst a larger number of MAC units. Table 1 shows that *S2TA-W* with a  $4 \times 4 \times 4_4 \times 8$  TPE

<sup>2</sup>Accumulator update is a read/modify/write: read destination register, add multiplier result(s), and write back to the same register.

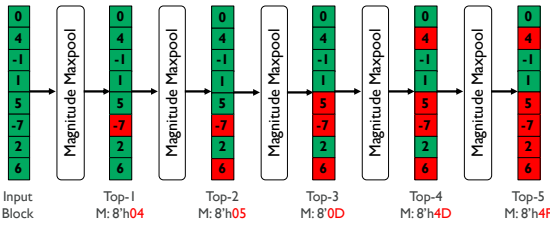


Figure 8: Hardware DAP array, consisting of cascaded magnitude (absolute value) maxpool stages, configured for an input block of  $BZ = 8$ , with  $NNZ \leq 5$ . The elements in red are discounted in consecutive maxpools. For 4/8 DBB, the output will be the elements  $[4, 5, -7, 6]$  and the positional bit mask  $M = 8'h4D$ .

array, and time-unrolled  $8 \times 4 \times 4\_8 \times 8$  S2TA-AW for  $BZ=8$  have  $\sim 7-1,886 \times$  less total buffers per MAC than previous architectures. As a result, a larger TPE would also increase the energy efficiency, albeit this must be balanced against a marginal critical path growth to achieve the target clock frequency. Moreover, without losing generality, the TPE working in outer-product would outperform the TPE with the dot-product operation due to more efficient data reuse.

## 6.2 Hardware Support for DAP

To support A-DBB, the hardware must implement DAP, which simply selects the  $NNZ$  activation elements with the largest magnitude from the  $BZ$ -block (Section 5.1).

The challenge of providing hardware support for DAP is that the  $NNZ$  in a A-DBB block is variable at run time. To support this, the DAP hardware cascades  $NNZ$  number of maxpool stages. Fig. 8 shows the DAP hardware. Each maxpool selects the largest magnitude elements from the input block through binary comparison using  $BZ - 1$  comparators, which in our current design is fixed to contain 8 elements as a block size of 8 is empirically found to provide a good balance between accuracy and efficiency (Sec. 8.1).

We cap the maxpool stages at 5, since higher  $NNZ$  would usually not lead to significant efficiency gains. Thus, the DAP hardware (Table 2) supports a A-DBB sparsity ratio ranging from  $1/8$  to  $5/8$ , bypassing any unused stages.

## 6.3 Other Design and Implementation Details

**On-chip SRAM** As is commonplace for accelerators, we heavily leverage local software managed SRAM [22] to provide a low-cost operand supply. The 0.5MB weight buffer (WB) and the 2MB activation buffer (AB) are separate. Both are double buffered to overlap computation in the TPE array and DMA data transfer. The SRAM is grouped, rather than distributed, so we can use large high density SRAMs.

**Local MCU with SIMD** We implement non-GEMM operations such as activation functions, pooling, scaling, normalization and data type casting using Arm Cortex-M33 [1] microcontrollers (MCUs), which have 32-bit SIMD instructions [2]. M33 is very small ( $0.008\text{mm}^2$  [1]) and low power ( $3.9\mu\text{W}/\text{MHz}$  [1]) in 16 nm. Control and data movement (DMA) tasks are also performed by the MCUs, e.g. loading the input image into AB. We use a cluster of 4 MCUs each with a small 64KB control store SRAM, which is sufficient to ensure that the MCUs are never the performance bottleneck.

Table 2: Area and power breakdown of the S2TA-A/W DBB design using a 16 nm process node,  $8 \times 4 \times 4\_8 \times 8$  TPE configuration for  $BZ = 8$ , with 4 TOPS peak (dense) throughput.

Component	Power, mW	Area, $\text{mm}^2$
MAC Datapath and Buffers	317.7 (58.7%)	0.72 (19.1%)
Weight SRAM (512KB)	69.4 (12.8%)	0.54 (14.3%)
Activation SRAM (2MB)	93.4 (17.2%)	2.16 (57.3%)
Cortex-M33 MCU [1] $\times 4$	50.4 (9.3%)	0.30 (8.0%)
DAP Array	10.4 (2%)	0.05 (1.3%)
Total	541.3 (100%)	3.77 (100%)

## 7. METHODOLOGY

**Automatic RTL Generation** The S2TA accelerator is highly modular and can be configured to make a calculated trade-off between area, performance, and power consumption. Instead of evaluating an arbitrary design point, we implement a parameterized Python RTL generator to explore the full design space, defined by five main parameters: the three TPE dimensions (A, B, C in Sec. 6.1) and the dimension of the entire SA (M, N); altogether denoted as  $A \times B \times C\_M \times N$ . Each design can be further configured with any combination of W-DBB, A-DBB, ZVCG, and time-unrolling.

The RTL generator produces synthesizable Verilog RTL, along with a testbench suite. Each design is automatically validated in Synopsys VCS using the generated testbench, which executes inference on a given CNN model. This generates accurate performance (throughput) metrics. During the simulation, we also log value change dump (VCD) switching activity traces used for accurate annotated power simulation.

**Physical Design and Evaluation** To evaluate area and power, each design goes through a complete EDA flow consisting of Synopsys and Cadence tools, with the TSMC PDKs and Arm multi-Vt cell libraries and single-ported SRAM compilers. We used both TSMC 16nm FinFET and TSMC 65nm technology. The clock frequency is constrained to 1GHz in 16nm (500MHz in 65nm) at the slow corner, with multiple process, voltage and temperature corners for setup and hold timing. Power analysis was performed at the typical corner, using Synopsys PrimeTimePX, with the parasitic-annotated netlist and switching activity from VCD simulation traces.

**S2TA-A/W Design Point** Based on typical mobile DNN accelerator specs, we set a hard constraint of 4 TOPS peak (dense) throughput and clock frequency of 1GHz in 16nm (500MHz in 65nm). We then sweep the design space to identify designs on the area-vs-power frontier, from which we identify the TPE array design with the lowest power, which is the  $8 \times 4 \times 4\_8 \times 8$  outer-product TPE implemented with the time-unrolled DP1M4 datapath (Fig. 6(e)). This configuration with 4/8 W-DBB and variable A-DBB is referred to as S2TA-AW, and is used throughout the evaluation. Full area and power breakdown of S2TA-AW is shown in Table 2.

**Baselines** We compare against the following baselines, summarized in Tbl. 5:

- **SA-ZVCG**: classic SA design with zero-value clock gating ( $1 \times 1 \times 1\_32 \times 64$  TPE array in our notation).
- **S2TA-W**: this is the variant of S2TA that exploits 4/8 W-DBB sparsity alone (dense activations), using a  $4 \times 8 \times 4\_4 \times 8$  TPE with 4-MAC dot-product datapaths

(DP4M8 in Fig. 6(c)). Comparing against S2TA-W allows us to understand the gains from exploiting A-DBB and W-DBB jointly. This design also implements ZVCG to weakly exploit activation sparsity.

- SA-SMT: our INT8 re-implementation of a recent systolic array design that exploits unstructured sparsity using operand staging FIFOs to distribute matching operands [35], using the T2Q2 variant from the paper.
- SPARTEN and EYERISS-v2: both are recent non-systolic array designs [5, 12] that exploit unstructured sparsity.

All systolic array designs have 4 TOPS peak (dense) throughput and otherwise have identical configurations. We use the same EDA flow to obtain the performance, power, and area (PPA) metrics for a fair comparison. The PPA metrics for non-systolic array-based designs, i.e. SparTen and Eyeriss-v2, are directly extracted from the original papers.

## 8. EVALUATION RESULTS

### 8.1 Accuracy Results

As with virtually all forms of sparsity, DBB sparsity used in S2TA is lossy, and thus requires DNN fine-tuning to regain any accuracy loss. Here, we first describe the simple extensions to the conventional DNN training procedure to support DBB sparsity, followed by the accuracy results. We evaluate INT8 models since we focus on mobile inference, where INT8 is the most widely used for deployment [36].

**Training for W-DBB** We apply magnitude based DBB-aware weight pruning, which is similar to random magnitude pruning [41], but pruning independently within each DBB block. This typically runs for 20-50 epochs, progressively pruning small-magnitude weights within each DBB block, until the desired DBB sparsity constraint is met.

Tbl. 3 shows the results of W-DBB (with dense activation) fine-tuning of five popular CNNs with INT8 quantization: VGG-16, MobileNetV1, ResNet-50V1 on ImageNet, and LeNet-5 on MNIST. We find that 4/8 W-DBB density typically achieves <0.5% accuracy loss, on both a relatively big network (ResNet-50V1) and a compact parameter-efficient network (MobileNetV1).

In general, a larger block size (BZ) relaxes accuracy loss, but increases the hardware cost to exploit the sparsity. Meanwhile, a larger NNZ per block increases accuracy while leaving less room for exploiting sparsity. This is evident as we increase the NNZ for ResNet-50V1 from 2 to 4 in Tbl. 3. Overall, we find that 4/8 DBB density level is a good compromise that achieves low accuracy loss for both compact models such as MobileNet and larger (older) models that are easier to prune. Compared to previous work, Kang [18] targets a fixed 2/8 W-DBB, which is too aggressive to achieve good accuracy, while the Nvidia A100 [25] uses 2/4, which is the same sparsity level as our 4/8 choice, but less flexible.

**Training for A-DBB** Dynamic Activation Pruning (DAP) is lossy and requires fine-tuning to minimize accuracy impact. We incorporate DAP into DNN fine-tuning by adding DAP in front of convolution operations, mimicking how it is used at inference. To back propagate through the DAP layer, we calculate the gradient of DAP with respect to the activation  $a$

Table 3: Accuracies of the baseline (INT8) models and various DBB variants. The accuracy loss of exploiting both A-DBB and W-DBB is generally about 1%. The accuracy loss of exploiting one form of sparsity is about 0.5%. A-DBB density varies significantly across layers. We report the weighted average, which can be a non-integer ratio.

Model	Dataset	Baseline <sup>3</sup> Acc. (%)	DBB Pruning		Acc. (%)
			A-DBB <sup>1</sup>	W-DBB <sup>2</sup>	
LeNet-5	MNIST	99.0	3/8	–	98.9
LeNet-5	MNIST	99.0	–	2/8	98.9
LeNet-5	MNIST	99.0	4/8	2/8	98.8
MobileNetV1	ImageNet	70.1	3.8/8	–	69.4
MobileNetV1	ImageNet	70.1	–	4/8	69.8
MobileNetV1 *	ImageNet	70.1	4.8/8	4/8	68.9
AlexNet	ImageNet	55.7	3.8/8	–	54.7
AlexNet	ImageNet	55.7	–	4/8	54.9
AlexNet *	ImageNet	55.7	3.9/8	4/8	54.6
VGG-16	ImageNet	71.5	3.1/8	–	71.8
VGG-16	ImageNet	71.5	–	3/8	71.4
VGG-16 *	ImageNet	71.5	3.1/8	3/8	71.9
ResNet-50V1	ImageNet	75.0	–	4/8	74.5
ResNet-50V1	ImageNet	75.0	–	3/8	74.3
ResNet-50V1	ImageNet	75.0	–	2/8	73.1
ResNet-50V1	ImageNet	75.0	3.49/8	–	74.4
ResNet-50V1 *	ImageNet	75.0	3.49/8	3/8	73.9
ResNet-50V1	ImageNet	75.0	3.49/8	4/8	74.1

<sup>1</sup>Tuned per-layer, average reported; and – for dense. <sup>2</sup>Tuned per-model (excluding the 1st layer); and – for dense. <sup>3</sup>8-bit dense models. \* Used for whole model evaluation in Sec. 8.3.

$\frac{\partial DAP(a)}{\partial a}$ , which is a binary mask tensor with a value 1 for the *Top-NNZ* elements and a value 0 for the pruned ones.

As an example, MobileNetV1 shows a test accuracy drop from 71% to 56.1% when using 4/8 A-DBB for all point-wise CNN layers before fine-tuning. A 30-epoch DAP-aware fine-tuning recovers the accuracy to 70.2%. We find that 50-100 epochs of fine-tuning are typically sufficient.

Tbl. 3 also shows the accuracy of applying A-DBB alone and applying both forms of DBB sparsity jointly. Note that while W-DBB density is hypertuned on a per-model basis, the A-DBB density varies wildly from early layers to later layers and is therefore tuned per-layer (supported by S2TA-AW). We observe that combined A/W-DBB has a 0.1%–0.4% accuracy loss compared to exploiting W-DBB alone. Total additional training time is less than 48 hours in all cases.

### 8.2 Microbenchmarking Results

We first use a set of synthetic (microbenchmark) DNNs with specific weight/activation sparsity to understand the performance, energy, and area of S2TA relative to the baselines.

Fig. 9a show show the energy and performance of SA-ZVCG vary with weight and activation density. The  $x$ -axis increases the weight sparsity from 0% to 87.5%, and the two bars refer to two different activation densities of 50% and 20%, respectively. The energy is normalized to energy per MAC operation. Naturally, the energy of SA-ZVCG scales weakly as the weight and activation sparsity increases due to the clock gating, but there is no speedup regardless of the sparsity. Fig. 9b shows that SA-SMT exploiting unstructured sparsity for both weight and activation consumes significant higher energy than the SA-ZVCG in Fig. 9a.

**Exploiting W-DBB Alone** Fig. 9c shows the energy and performance of S2TA-W normalized to SA-ZVCG. S2TA-W

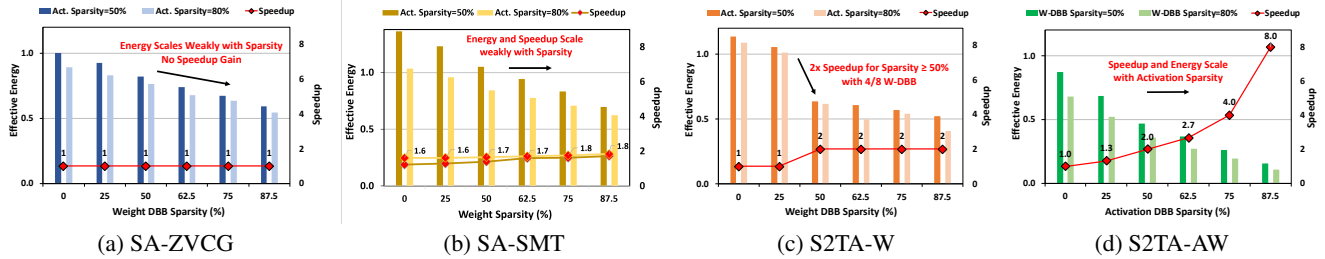


Figure 9: Energy (normalized to SA-ZVCG at 0% activation and 50% weight sparsity) and speedup with sparsity. (a) SA-ZVCG energy falls slowly with density, no speedup. (b) SA-SMT shows higher energy than SA-ZVCG, up to  $2\times$  speedup. (c) S2TA-W exploiting W-DBB alone provides a fixed  $2\times$  speedup with negligible overheads, and hence close  $2\times$  energy reduction compared to dense, at sparsity  $\geq 50\%$ . (d) S2TA-AW with A/W-DBB exploits joint sparsity for up to  $8\times$  speedup and very significant energy reduction.

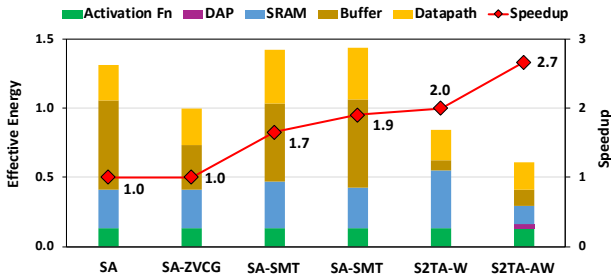


Figure 10: Energy breakdown and speedup of various SA variants for a typical convolution with 50% (4/8-DBB) and 62.5% (3/8-DBB) INT8 weight and activation sparsity, respectively. The results are normalized to SA-ZVCG.

exploits a 4/8 W-DBB sparsity and, thus, achieves a maximal  $2\times$  speedup step when weight sparsity is  $\geq 50\%$ . The  $2\times$  speedup also gives a corresponding energy reduction. However, the energy reduction at 50% weight sparsity then plateaus, only scaling weakly with additional DBB weight sparsity and lower switching activity. Clearly, S2TA-W cannot maximally exploit the abundant activation sparsity.

**Exploiting A/W-DBB Jointly** Exploiting both forms of sparsity, Fig. 9d shows that S2TA-AW achieves a very significant energy reduction of up to  $9.1\times$  compared to SA-ZVCG.

While the speedup from S2TA-W is capped at  $2\times$  regardless of the activation sparsity, S2TA-AW supports variable activation compression and so the speedup increases with activation sparsity from  $1\times$  at dense to  $8\times$  at 12.5% activation density. As discussed in Sec. 5.2, the ability to exploit variable activation sparsity is essential as the activation density varies significantly across the layers of a DNN.

**Compared to Exploiting Unstructured Sparsity** Fig. 10 shows energy (left y-axis) and speedup (right y-axis) on a typical convolution layer with 50% weight and 62.5% activation sparsity across the baseline SA variants (SA, SA-ZVCG, S2TA-W) and SA-SMT [35], which is a SA-based accelerator exploiting unstructured sparsity using staging FIFOs with same INT8 operands. The results are normalized to SA-ZVCG. We also break down the energy consumption into different components: the datapath of the PE array, the buffers in the PE array, SRAM, activation layers (M33), and the DAP logic, which is unique to S2TA-AW. We evaluate two variants of SA-SMT: T2Q2 has an operand staging

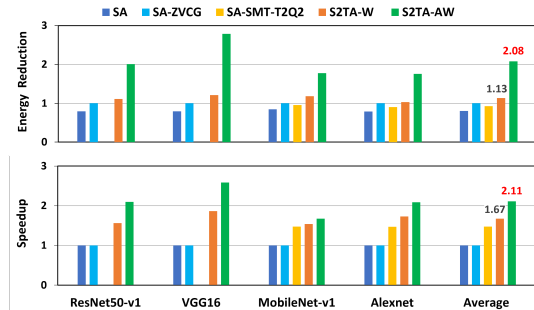


Figure 11: Energy reduction and speedup (normalized to SA-ZVCG) comparison on ResNet50V1, VGG16, MobileNetV1, and AlexNet (Convolution only). All data is obtained using the same 16nm technology. The S2TA-AW is  $2.08\times$ ,  $1.84\times$ , and  $2.24\times$  energy efficient, and  $2.11\times$ ,  $1.26\times$ , and  $1.43\times$  speedup than SA-ZVCG, S2TA-W, and SA-SMT baselines, respectively.

FIFO depth of two and T2Q4 has FIFO depth 4.

While both SA-SMT variants are faster than SA-ZVCG, they both also increase the effective energy consumption by 43.0% (T2Q2) and 41.2% (T2Q4) compared to the baseline SA-ZVCG. This is due to the energy overhead of the staging buffer for distributing matched operands, which is not necessary for S2TA-W and S2TA-AW. This is further evident in the significantly lower buffering energy for S2TA-W and S2TA-AW in Fig. 10.

A closer comparison between S2TA-W and S2TA-AW in Fig. 10 shows that the energy benefits of S2TA-AW mainly come from a  $3.1\times$  reduction in the SRAM energy, because S2TA-AW exploits activation sparsity using the time-unrolled outer-product TPE array, whereas S2TA-W loads redundant (zero) activations from SRAM.

### 8.3 Full Model Inference Results

We compare S2TA-AW with SA, SA-ZVCG, SA-SMT, and S2TA-W across four models: VGG16, MobileNetv1, ResNet50v1, and AlexNet. Fig. 11 gives energy reduction (top figure) and speedup (bottom figure) comparison, normalized to SA-ZVCG. Compared to SA-ZVCG, S2TA-AW reduces energy by 1.76–2.79 $\times$ , with 1.67–2.58 $\times$  speedup.

**S2TA-W** On average, S2TA-AW consumes 1.84 $\times$  lower energy and achieves 1.26 $\times$  speedup over S2TA-W (Fig. 11).

Table 4: Comparison of S2TA-AW and baselines, along with previously published sparse CNN accelerators in 16nm/65nm.

	<u>SparTen</u> [12]	<u>Eyeriss v2</u> [5]	<u>SA-ZVCG</u> <sup>1</sup>	<u>SA-SMT</u> <sup>1</sup> [35]	<u>S2TA-W</u> <sup>1</sup>	<u>S2TA-AW</u> <sup>1</sup>
<b>Weight Sparsity</b>	Random	Random	ZVCG	Random	4/8 DBB, Dense	4/8 DBB, Dense
<b>Activation Sparsity</b>	Random	Random	ZVCG	Random	Dense	1/8-5/8 DBB, Dense
<b>SRAM Size (W/A)</b>	-	246KB	2MB / 0.5MB	2MB / 0.5MB	2MB / 0.5MB	2MB / 0.5MB
<b>Hardware MACs</b>	32 (INT8)	384 (INT8)	2048 (INT8)	2048 (INT8)	2048 (INT8)	2048 (INT8)
<b>Process Technology</b>	16nm					
<b>Clock Freq.</b>	GHz	-	1.0	1.0	1.0	1.0
<b>Area</b>	mm <sup>2</sup>	-	3.7	4.2	3.4	3.8
<b>Peak Throughput</b> <sup>2</sup>	TOPS	-	4	8	8	8 (16 <sup>6</sup> )
<b>Peak Energy Eff.</b> <sup>2</sup>	TOPS/W	-	10.5 (12.8 <sup>3</sup> )	8.01 (11.9 <sup>3</sup> )	12.4 (13.9 <sup>3</sup> )	14.3 (26.5 <sup>3</sup> )
	$\times 10^3$ Inf./sec	-	2.2 (3.0 <sup>5</sup> )	2.7 (4.0 <sup>5</sup> )	3.3 (5.0 <sup>5</sup> )	3.7 (6.3 <sup>5</sup> )
<b>AlexNet</b>	$\times 10^3$ Inf./J	-	4.81 (7.5 <sup>5</sup> )	4.48 (6.73 <sup>5</sup> )	7.2 (8.7 <sup>5</sup> )	9.9 (13.1 <sup>5</sup> )
	TOPS/W	-	7.2 (9.8 <sup>5</sup> )	6.7 (8.7 <sup>5</sup> )	9.8 (11 <sup>5</sup> )	14 (19 <sup>5</sup> )
	$\times 10^3$ Inf./sec	-	2.7 (3.6 <sup>5</sup> )	3.5 (5.4 <sup>5</sup> )	4.2 (7.3 <sup>5</sup> )	5.2 (9.7 <sup>5</sup> )
<b>MobileNet</b>	$\times 10^3$ Inf./J	-	7.9 (8.4 <sup>5</sup> )	7.5 (8.0 <sup>5</sup> )	9.2 (9.9 <sup>5</sup> )	13.3 (14.9 <sup>5</sup> )
	TOPS/W	-	8.7 (9.2 <sup>5</sup> )	8.2 (9.0 <sup>5</sup> )	10 (11 <sup>5</sup> )	14 (17 <sup>5</sup> )
<b>Process Technology</b>	45nm	65nm	65nm	-	65nm	65nm
<b>Clock Freq.</b>	GHz	0.8	0.2	0.5	0.5	0.5
<b>Area</b>	mm <sup>2</sup>	0.766 <sup>6</sup>	3.38 <sup>6,7</sup>	21	-	24
<b>Peak Throughput</b> <sup>2</sup>	TOPS	0.2	0.152	2	-	4 (8 <sup>6</sup> )
<b>Peak Energy Eff.</b> <sup>2</sup>	TOPS/W	-	-	0.78	-	0.87
	$\times 10^3$ Inf./sec	-	0.28 (0.34 <sup>5</sup> )	1.1 (1.5 <sup>5</sup> )	-	1.6 (2.5 <sup>5</sup> )
<b>AlexNet</b>	$\times 10^3$ Inf./J	(0.52 <sup>5</sup> )	0.66 (0.74 <sup>5</sup> )	0.44 (0.67 <sup>5</sup> )	-	0.55 (0.66 <sup>5</sup> )
	TOPS/W	(0.68 <sup>5</sup> )	0.96 (1.1 <sup>5</sup> )	0.67 (0.95 <sup>5</sup> )	-	0.82 (0.95 <sup>5</sup> )
	$\times 10^3$ Inf./sec	-	0.13 <sup>4</sup>	1.6 (1.82 <sup>5</sup> )	-	1.82 (3.64 <sup>5</sup> )
<b>MobileNet</b>	$\times 10^3$ Inf./J	-	0.22 <sup>4</sup>	0.68	-	0.76
	TOPS/W	-	0.24	0.75	-	0.83

<sup>1</sup>Our results. <sup>2</sup>50% sparse weights and activations. <sup>3</sup>75% sparse weights and activations. <sup>4</sup>Scaled from MobileNet-v1-0.5-128 to 1.0-224. <sup>5</sup>Conv only. <sup>6</sup>Logic only. <sup>7</sup>2.7Mgates.

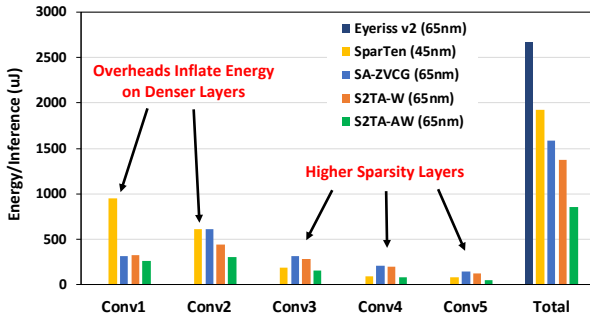


Figure 12: AlexNet per-layer energy for EYERISS-V2 [5], SPARTEN [12], SA-ZVCG, S2TA-W, and the optimal S2TA-AW. S2TA-AW in 65nm is about 2.2 $\times$  more efficient than the 45nm SPARTEN on AlexNet energy per inference. SparTen has low energy only on very high sparsity layers (i.e. Conv3, 4 and 5). EYERISS-V2 consumes 3.1 $\times$  more total energy than S2TA-AW in the same 65nm technology. Note, per-layer energy is not reported in Eyeriss-v2 [5].

**SA-SMT** S2TA is the first systolic architecture to exploit DBB sparsity. SA-SMT [35] exploits unstructured sparsity in a systolic array accelerator. SA-SMT suffers from the overhead of distributing matching pairs, which can stall the data flow in the systolic array, which SA-SMT resolves using expensive operand buffer FIFOs (Sec. 2.2). We reimplemented SA-SMT, which achieves 8.01 TOPS/W compared to 14.3 TOPS/W for S2TA-AW at the same sparsity, as shown in Tbl. 4. This is due to the high cost of the additional FIFOs, which quickly dominate energy (Fig. 9b and 10).

**Non-SA Accelerators** We now compare S2TA with two non-SA accelerators, SPARTEN and EYERISS-V2, both of which exploit unstructured sparsity.

SPARTEN [12] is a state-of-the-art CNN accelerator that exploits unstructured sparsity in weights and activations, with superior results to SCNN [27]. For the comparison, we reimplemented S2TA-AW in 65nm technology (previous results are all in 16nm), which is older than the 45nm used for SPARTEN and, thus, does not unfairly favor S2TA-AW. Fig. 12 compares the energy per inference for S2TA-AW and SPARTEN on AlexNet, with SA-ZVCG and S2TA-W. The total energy per inference on AlexNet is 2.2 $\times$  lower on S2TA-AW compared to SPARTEN, even with a one node process disadvantage (65nm vs 45nm). The gain on MobileNet is even greater, as shown in Tbl. 4. A closer examination shows that SPARTEN performs best on layers with very high sparsity (e.g., Conv3-5), and less well on layers with dense or more moderate sparsity (e.g., Conv1,2).

A comparison with EYERISS-V2 [5] is given in Tbl. 4 and Fig. 12. S2TA-AW shows 4.7 $\times$  and 1.4 $\times$  higher energy efficiency on MobileNet and AlexNet for convolution layers, respectively, compared to EYERISS-V2. Fig. 12 indicates EYERISS-V2 is 3.1 $\times$  less energy efficient than S2TA-AW in the same 65 nm process technology.

These results demonstrate that although the speedup gained by S2TA with full DBB sparsity is moderate, the overheads are so low that the overall architecture is more energy efficient. In fact, we find that even the baseline SA-ZVCG has lower energy than SPARTEN on AlexNet and EYERISS-V2 on MobileNet. While achieving high speedup from sparsity is important for certain scenarios, it is essential to also consider the overheads and start with an efficient architecture template, which is especially important for mobile inference.

## 8.4 Summary of Results

Finally, we summarize the key results. Based on full-

accelerator synthesis data, on a typical convolution layer with 50–75% weight and activation sparsity range, the 16nm S2TA-AW achieves 8-16 TOPS throughput, 14.3–26.5 TOPS/W power efficiency, and 2.16–4.21 TOPS/mm<sup>2</sup> area efficiency.

On a range of popular DNN models (including both relatively big models such as ResNet-50V1 and compact parameter-efficient models such as MobileNetV1), S2TA-AW achieves an average 2.08× energy reduction and 2.11× speedup compared to SA-ZVCG, which itself consumes 25% less energy compared to a dense SA. S2TA-W exploiting W-DBB alone only marginally reduces energy (by 1.13×) compared to the SA-ZVCG baseline, which emphasizes the importance of the time-unrolled architecture for jointly exploiting weight and activation DBB sparsity. S2TA-AW also achieves 1.4–4.7× lower energy than state-of-the-art accelerators exploiting unstructured sparsity, including SPARTEN, EYERISSV2, and SA-SMT. Table 5 summarizes key aspects of this work.

As with any SA-based inference accelerators, fully-connected (FC) and depthwise (DW) layers are memory bound on S2TA, as batching is typically not used in inference. However, we do prune FC/DW, included in the full model results in Tbl. 4.

## 9. RELATED WORK

**Zero Value Clock Gating (ZVCG)** (Sec. 2.1) saves power when one or more zero operands are encountered [6, 17, 30]. We apply ZVCG to exploit excess sparsity that cannot be fully exploited by DBB.

**Indexed Unstructured Sparsity** EIE [14] implements a fine-grained unstructured sparse CSR-encoded INT16 matrix-vector accelerator for dense layers, and ESE [15] extends this to LSTMs. MASR [13] also exploits unstructured sparsity for RNNs, but uses a bitmask encoding. A number of papers target unstructured sparse matrix multiplication for very sparse data, such as Outer Space [26], which uses an outer product scheme, and SpArch [39], which further optimizes for locality. More specific to the lower sparsity of CNNs, Cnvlutin [4] skips compute for zero activations, without explicit indexes. SCNN [27] implements a fully CSR-indexed sparse CNN accelerator using an outer product to exploit sparse weights and activations. FixyNN [38] demonstrates a fixed-weight accelerator that can very efficiently exploit random sparsity. SparTen [12] and Eyeriss v2 [5] both support fully-sparse inference. We focus on DBB sparsity, but compare and contrast with SparTen, and Eyeriss v2 in (Table 4).

**DBB Sparsity** Kang [18] implements accelerator exploiting a fixed 2/8 W-DBB sparsity. The accelerator design is also based on a dot product microarchitecture with limited data reuse. Similar work [40] also exploited W-DBB in the GPU context. Nvidia’s proprietary A100 GPU design exploits fixed 2/4 W-DBB INT8 structured sparsity with 3.12 TOPS/W [7] (peak), which is 4× lower than the 12.4 TOPS/W of our S2TA-W baseline in Table 4, achieves up to 1.5× speedup for INT8 model, while the theoretical speedup is 2× [25, 28]. S2TA is the first architecture exploiting both W-DBB and A-DBB, and is the first to incorporate DBB into a systolic array with the novel time-unrolled technique exploiting new dimensions of data reuse for up to 8× peak speedup.

**Sparsity in Systolic Arrays** SAs like the Google TPU [17] are efficient because they have high data reuse and local communication. SMT-SA [35] is an SA that exploits unstructured

Table 5: Summary of designs evaluated in this paper and previous works. S2TA-AW demonstrates a very low overhead fully-sparse architecture that achieves significant speedup and energy efficiency gains.

Architecture	Weight Sparsity	Activation Sparsity	ZVCG	Time-Unrolled Variable DBB
Nvidia A100 [25]	DBB	×	– <sup>1</sup>	×
Kang et al. [18]	DBB	×	×	×
SA [17]	×	×	×	×
SA-ZVCG	×	×	✓	×
SA-SMT [35]	Random	Random	✓	×
S2TA-W	DBB	×	×	×
S2TA-AW	DBB	DBB	✓	✓

<sup>1</sup> Unpublished proprietary design.

sparsity using data staging FIFOs in the array, which are energy inefficient for INT8 datapath, although acceptable for FP32 [24, 35]. Kung et al. [21] showed a preprocessing step of column combining of sparse weight matrices, before processing on a dense SA architecture. Liu et al. [23] exploited W-DBB sparsity in systolic architecture. NB-SMT [34] is a sparse SA with the ability to momentarily halve the MAC precision to match the throughput requirement. This can potentially be combined with DBB, although it leads to unpredictable accuracy at run time.

**Bit-wise Sparsity** Even sign extension and zero bits within a word can be considered for optimization: Pragmatic [3] implements weight bit-sparsity, Tactical [8] implements activation bit-sparsity, and Laconic [33] implements weight and activation bit-sparsity. While orthogonal to our work, bit-sparsity is an interesting avenue for future DBB research.

## 10. CONCLUSION

Density bound block (DBB) sparsity is a powerful approach to exploit CNN sparsity, without the overheads of random sparsity schemes. While DBB has previously been introduced in a limited form to exploit weight sparsity, this paper describes an architecture to exploit DBB sparsity on both weight and activation. For weight DBB, we can implement pruning during training to ensure the data meets the DBB constraint. However, we cannot do this for activations, which are not static, but rather calculated at runtime. Therefore to implement activation DBB, we introduce a co-design solution - Dynamic Activation Pruning (DAP) in hardware during runtime to force the required DBB sparsity. This process is lossy and therefore must also be incorporated during the training of the model, to prevent accuracy loss for inference.

The proposed novel time-unrolled DBB sparsity architecture, S2TA-AW implemented joint weight and activation sparsity in an efficient systolic architecture. The design significantly outperforms other implemented comparison baselines shown in Tbl. 5, including variants S2TA-W and SA-SMT, which exploit weight DBB sparsity alone and fully unstructured sparsity, respectively. On the pruned INT8 benchmark models AlexNet, MobileNetv1, VGG16, ResNet50v1, a 16nm S2TA-AW with joint weight and activation DBB sparsity demonstrates 2.08× and 1.84× energy reduction, on average, compared to the baseline SA-ZVCG and S2TA-W which exploits weight DBB sparsity alone, respectively. Finally, S2TA-AW has about 2× and 3× the energy efficiency of the state-of-the-art unstructured sparse accelerator SparTen and Eyeriss-v2 on AlexNet, respectively.

## REFERENCES

- [1] Arm Cortex-M33. [Online]. Available: <https://developer.arm.com/ip-products/processors/cortex-m/cortex-m33>
- [2] ARMv8-M Architecture Reference Manual. [Online]. Available: [https://static.docs.arm.com/ddi0553/a/DDI0553A\\_e\\_armv8m\\_arm.pdf](https://static.docs.arm.com/ddi0553/a/DDI0553A_e_armv8m_arm.pdf)
- [3] J. Albericio, A. Delmás, P. Judd, S. Sharify, G. O’Leary, R. Genov, and A. Moshovos, “Bit-pragmatic deep neural network computing,” in *Proceedings of the 50th Annual IEEE/ACM International Symposium on Microarchitecture*, ser. MICRO-50 ’17. New York, NY, USA: Association for Computing Machinery, 2017, p. 382–394. [Online]. Available: <https://doi.org/10.1145/3123939.3123982>
- [4] J. Albericio, P. Judd, T. Hetherington, T. Aamodt, N. E. Jeger, and A. Moshovos, “Cnvlutin: Ineffective-neuron-free deep neural network computing,” in *Proceedings of the 43rd International Symposium on Computer Architecture*, ser. ISCA ’16. Piscataway, NJ, USA: IEEE Press, 2016, pp. 1–13. [Online]. Available: <https://doi.org/10.1109/ISCA.2016.11>
- [5] Y. Chen, T. Yang, J. Emer, and V. Sze, “Eyeriss v2: A flexible accelerator for emerging deep neural networks on mobile devices,” *IEEE Journal on Emerging and Selected Topics in Circuits and Systems*, vol. 9, no. 2, pp. 292–308, 2019.
- [6] Y.-H. Chen, J. Emer, and V. Sze, “Eyeriss: A spatial architecture for energy-efficient dataflow for convolutional neural networks,” in *Proceedings of the 43rd International Symposium on Computer Architecture*. Piscataway, NJ, USA: IEEE Press, 2016, pp. 367–379. [Online]. Available: <https://doi.org/10.1109/ISCA.2016.40>
- [7] B. Dally. Logarithmic numbers and asynchronous accumulators, the future of dl chips. MLSYS2021. [Online]. Available: [https://media.mlsys.org/Conferences/MLSYS2021/Slides/DL\\_Chips\\_ML\\_Sys\\_0421.pdf](https://media.mlsys.org/Conferences/MLSYS2021/Slides/DL_Chips_ML_Sys_0421.pdf)
- [8] A. Delmas Lascorz, P. Judd, D. M. Stuart, Z. Poulos, M. Mahmoud, S. Sharify, M. Nikolic, K. Siu, and A. Moshovos, “Bit-tactical: A software/hardware approach to exploiting value and bit sparsity in neural networks,” in *Proceedings of the Twenty-Fourth International Conference on Architectural Support for Programming Languages and Operating Systems*, ser. ASPLOS ’19. New York, NY, USA: Association for Computing Machinery, 2019, p. 749–763. [Online]. Available: <https://doi.org/10.1145/3297858.3304041>
- [9] I. Fedorov, R. P. Adams, M. Mattina, and P. N. Whatmough, “SpArSe: Sparse architecture search for CNNs on resource-constrained microcontrollers,” in *Advances in Neural Information Processing Systems (NeurIPS)*, 2019, pp. 4978–4990.
- [10] I. Fedorov, M. Stamenovic, C. Jenson, L.-C. Yang, A. Mandell, Y. Gan, M. Mattina, and P. N. Whatmough, “TinyLSTMs: Efficient Neural Speech Enhancement for Hearing Aids,” in *Conference of the International Speech Communication Association (INTERSPEECH)*, 2020.
- [11] Y. Feng, P. Whatmough, and Y. Zhu, “ASV: Accelerated Stereo Vision System,” in *Proceedings of the 52nd Annual IEEE/ACM International Symposium on Microarchitecture*, ser. MICRO ’52. New York, NY, USA: Association for Computing Machinery, 2019, p. 643–656. [Online]. Available: <https://doi.org/10.1145/3352460.3358253>
- [12] A. Gondimalla, N. Chesnut, M. Thottethodi, and T. N. Vijaykumar, “Sparten: A sparse tensor accelerator for convolutional neural networks,” in *Proceedings of the 52nd Annual IEEE/ACM International Symposium on Microarchitecture*, ser. MICRO ’52. New York, NY, USA: Association for Computing Machinery, 2019, p. 151–165. [Online]. Available: <https://doi.org/10.1145/3352460.3358291>
- [13] U. Gupta, B. Reagen, L. Pentecost, M. Donato, T. Tambe, A. M. Rush, G. Wei, and D. Brooks, “MASR: A modular accelerator for sparse rnns,” in *28th International Conference on Parallel Architectures and Compilation Techniques, PACT 2019, Seattle, WA, USA, September 23-26, 2019*. IEEE, 2019, pp. 1–14. [Online]. Available: <https://doi.org/10.1109/PACT.2019.00009>
- [14] S. Han *et al.*, “EIE: Efficient inference engine on compressed deep neural network,” in *Proceedings of the 43rd Int. Symp. on Computer Architecture (ISCA)*, 2016.
- [15] S. Han, J. Kang, H. Mao, Y. Hu, X. Li, Y. Li, D. Xie, H. Luo, S. Yao, Y. Wang, H. Yang, and W. B. J. Dally, “Ese: Efficient speech recognition engine with sparse lstm on fpga,” in *Proceedings of the 2017 ACM/SIGDA International Symposium on Field-Programmable Gate Arrays*, ser. FPGA ’17. New York, NY, USA: Association for Computing Machinery, 2017, p. 75–84. [Online]. Available: <https://doi.org/10.1145/3020078.3021745>
- [16] P. Hansen, A. Vilkin, Y. Khurstalev, J. Imber, D. Hanwell, M. Mattina, and P. N. Whatmough, “ISP4ML: Understanding the Role of Image Signal Processing in Efficient Deep Learning Vision Systems,” in *International Conference on Pattern Recognition (ICPR)*, 2020.
- [17] N. P. Jouppi, C. Young, N. Patil, D. Patterson, G. Agrawal, R. Bajwa, S. Bates, S. Bhatia, N. Boden, A. Borchers, R. Boyle, P. Cantin, C. Chao, C. Clark, J. Coriell, M. Daley, M. Dau, J. Dean, B. Gelb, T. V. Ghaemmaghami, R. Gottipati, W. Gulland, R. Hagmann, R. C. Ho, D. Hogberg, J. Hu, R. Hundt, D. Hurt, J. Ibarz, A. Jaffey, A. Jaworski, A. Kaplan, H. Khaitan, A. Koch, N. Kumar, S. Lacy, J. Laudon, J. Law, D. Le, C. Leary, Z. Liu, K. Lucke, A. Lundin, G. MacKean, A. Maggiore, M. Mahony, K. Miller, R. Nagarajan, N. Narayanaswami, R. Ni, K. Nix, T. Norrie, M. Omernick, N. Penukonda, A. Phelps, J. Ross, A. Salek, E. Samadiani, C. Severn, G. Sizikov, M. Snellman, J. Souter, D. Steinberg, A. Swing, M. Tan, G. Thorson, B. Tian, H. Toma, E. Tuttle, V. Vasudevan, R. Walter, W. Wang, E. Wilcox, and D. H. Yoon, “In-datacenter performance analysis of a tensor processing unit,” *CoRR*, vol. abs/1704.04760, 2017. [Online]. Available: <http://arxiv.org/abs/1704.04760>
- [18] H. Kang, “Accelerator-aware pruning for convolutional neural networks,” *IEEE Transactions on Circuits and Systems for Video Technology*, pp. 1–1, 2019.
- [19] S. Kodali, P. Hansen, N. Mulholland, P. Whatmough, D. Brooks, and G. Wei, “Applications of Deep Neural Networks for Ultra Low Power IoT,” in *2017 IEEE International Conference on Computer Design (ICCD)*, 2017, pp. 589–592.
- [20] Kung, “Why systolic architectures?” *Computer*, vol. 15, no. 1, pp. 37–46, 1982.
- [21] H. Kung, B. McDanel, and S. Q. Zhang, “Packing sparse convolutional neural networks for efficient systolic array implementations: Column combining under joint optimization,” in *24th Int. Conf. on Architectural Support for Programming Languages and Operating Systems (ASPLOS)*, 2019, pp. 821–834.
- [22] H. Li, M. Bhargava, P. N. Whatmough, and H. Philip Wong, “On-chip memory technology design space explorations for mobile deep neural network accelerators,” in *2019 56th ACM/IEEE Design Automation Conference (DAC)*, 2019, pp. 1–6.
- [23] Z. Liu, P. N. Whatmough, and M. Mattina, “Systolic Tensor Array: An Efficient Structured-Sparse GEMM Accelerator for Mobile CNN Inference,” *IEEE Computer Architecture Letters*, vol. 19, no. 1, pp. 34–37, 2020.
- [24] M. Mahmoud, I. Edo, A. H. Zadeh, O. Mohamed Awad, G. Pekhimenko, J. Albericio, and A. Moshovos, “Tensordash: Exploiting sparsity to accelerate deep neural network training,” in *2020 53rd Annual IEEE/ACM International Symposium on Microarchitecture (MICRO)*, 2020, pp. 781–795.
- [25] Nvidia. A100 GPU Datasheet. [Online]. Available: <https://www.nvidia.com/content/dam/en-zz/Solutions/Data-Center/a100/pdf/nvidia-a100-datasheet.pdf>
- [26] S. Pal *et al.*, “Outerspace: An outer product based sparse matrix multiplication accelerator,” in *Int. Symp. on High Performance Computer Architecture (HPCA)*, Feb 2018, pp. 724–736.
- [27] A. Parashar *et al.*, “SCNN: An accelerator for compressed-sparse convolutional neural networks,” in *2017 ACM/IEEE 44th Annual International Symposium on Computer Architecture (ISCA)*, June 2017, pp. 27–40.
- [28] J. Pool. ACCELERATING SPARSITY IN THE NVIDIA AMPERE ARCHITECTURE. [Online]. Available: <https://developer.download.nvidia.com/video/gputechconf/gtc/2020/presentations/s22085-accelerating-sparsity-in-the-nvidia-ampere-architecture%E2%80%8B.pdf>
- [29] E. Qin, A. Samajdar, H. Kwon, V. Nadella, S. Srinivasan, D. Das, B. Kaul, and T. Krishna, “Sigma: A sparse and irregular gemm accelerator with flexible interconnects for dnn training,” in *2020 IEEE International Symposium on High Performance Computer Architecture (HPCA)*, 2020, pp. 58–70.
- [30] B. Reagen, P. Whatmough, R. Adolf, S. Rama, H. Lee, S. K. Lee, J. M. Hernández-Lobato, G.-Y. Wei, and D. Brooks, “Minerva: Enabling low-power, highly-accurate deep neural network accelerators,” in *Proceedings of the 43rd International Symposium on Computer Architecture*, ser. ISCA, 2016.

- [31] A. Samajdar, J. M. Joseph, Y. Zhu, P. Whatmough, M. Mattina, and T. Krishna, "A systematic methodology for characterizing scalability of dnn accelerators using scale-sim," in *2020 IEEE International Symposium on Performance Analysis of Systems and Software (ISPASS)*, 2020, pp. 58–68.
- [32] A. Samajdar, Y. Zhu, P. Whatmough, M. Mattina, and T. Krishna, "Scale-sim: Systolic cnn accelerator simulator," *arXiv preprint arXiv:1811.02883*, 2018.
- [33] S. Sharify, A. D. Lascorz, M. Mahmoud, M. Nikolic, K. Siu, D. M. Stuart, Z. Poulos, and A. Moshovos, "Laconic deep learning inference acceleration," in *Proceedings of the 46th International Symposium on Computer Architecture*, ser. ISCA '19. New York, NY, USA: Association for Computing Machinery, 2019, p. 304–317. [Online]. Available: <https://doi.org/10.1145/3307650.3322255>
- [34] G. Shomron and U. Weiser, "Non-blocking simultaneous multithreading: Embracing the resiliency of deep neural networks," in *2020 53rd Annual IEEE/ACM International Symposium on Microarchitecture (MICRO)*, 2020, pp. 256–269.
- [35] G. Shomron, T. Horowitz, and U. Weiser, "SMT-SA: Simultaneous multithreading in systolic arrays," *IEEE Comput. Archit. Lett.*, vol. 18, no. 2, pp. 99–102, Jul. 2019.
- [36] P. Warden. Why are eight bits enough for deep neural networks? [Online]. Available: <https://petewarden.com/2015/05/23/why-are-eight-bits-enough-for-deep-neural-networks/>
- [37] P. N. Whatmough, S. K. Lee, M. Donato, H. Hsueh, S. Xi, U. Gupta, L. Pentecost, G. G. Ko, D. Brooks, and G. Wei, "A 16nm 25mm<sup>2</sup> SoC with a 54.5x Flexibility-Efficiency Range from Dual-Core Arm Cortex-A53 to eFPGA and Cache-Coherent Accelerators," in *2019 Symposium on VLSI Circuits*, 2019, pp. C34–C35.
- [38] P. N. Whatmough, C. Zhou, P. Hansen, S. K. Venkataramanaiah, J. sun Seo, and M. Mattina, "FixyNN: Efficient Hardware for Mobile Computer Vision via Transfer Learning," in *Proceedings of the 2nd SysML Conference, Palo Alto, CA, USA*, 2019.
- [39] Z. Zhang, H. Wang, S. Han, and W. J. Dally, "Sparch: Efficient architecture for sparse matrix multiplication," in *26th IEEE International Symposium on High Performance Computer Architecture (HPCA)*, 2020.
- [40] M. Zhu, T. Zhang, Z. Gu, and Y. Xie, "Sparse tensor core: Algorithm and hardware co-design for vector-wise sparse neural networks on modern gpus," in *Proceedings of the 52nd Annual IEEE/ACM International Symposium on Microarchitecture*, ser. MICRO '52. New York, NY, USA: Association for Computing Machinery, 2019, p. 359–371. [Online]. Available: <https://doi.org/10.1145/3352460.3358269>
- [41] M. Zhu and S. Gupta, "To prune, or not to prune: exploring the efficacy of pruning for model compression," *CoRR*, vol. abs/1710.01878, 2017. [Online]. Available: <http://dblp.uni-trier.de/db/journals/corr/corr1710.html#abs-1710-01878>
- [42] Y. Zhu, A. Samajdar, M. Mattina, and P. Whatmough, "Euphrates: Algorithm-SoC Co-Design for Low-Power Mobile Continuous Vision," in *Proceedings of the 45th Annual International Symposium on Computer Architecture*, ser. ISCA '18. IEEE Press, 2018, p. 547–560. [Online]. Available: <https://doi.org/10.1109/ISCA.2018.00052>